The Astronomical Journal, 145:20 (15pp), 2013 January doi:10.1088/0004-6256/145/1/20

VERY-LOW-MASS STELLAR AND SUBSTELLAR COMPANIONS TO SOLAR-LIKE STARS FROM MARVELS. III. A SHORT-PERIOD BROWN DWARF CANDIDATE AROUND AN ACTIVE G0IV SUBGIANT

Bo Ma (馬波)[1], Jian Ge[1], Rory Barnes[2], Justin R. Crepp[3,4], Nathan De Lee[1,5], Leticia Dutra-Ferreira[6,7], Massimiliano Esposito[8,9], Bruno Femenia[8,9], Scott W. Fleming[1,10,11], B. Scott Gaudi[12], Luan Ghezzi[7,13], Leslie Hebb[5], Jonay I. Gonzalez Hernandez[8,9], Brian L. Lee[1,2], G. F. Porto de Mello[6,7], Keivan G. Stassun[5,14], Ji Wang[1], John P. Wisniewski[15], Eric Agol[2], Dmitry Bizyaev[16], Phillip Cargile[5], Liang Chang[1], Luiz Nicolaci da Costa[7,13], Jason D. Eastman[12,17,18], Bruce Gary[5], Peng Jiang[1], Stephen R. Kane[19], Rui Li[1], Jian Liu[1], Suvrath Mahadevan[1,10,11], Marcio A. G. Maia[7,13], Demitri Muna[20], Duy Cuong Nguyen[1], Ricardo L. C. Ogando[7,13], Daniel Oravetz[16], Joshua Pepper[5], Martin Paegert[5], Carlos Allende Prieto[8,9], Rafael Rebolo[8,21], Basilio X. Santiago[7,22], Donald P. Schneider[10,11], Alaina Shelden[16], Audrey Simmons[16], Thirupathi Sivarani[1,23], J. C. van Eyken[18,19], Xiaoke Wan[1], Benjamin A. Weaver[20], and Bo Zhao[1]

[1] Department of Astronomy, University of Florida, 211 Bryant Space Science Center, Gainesville, FL 32611-2055, USA; boma@astro.ufl.edu
[2] Department of Astronomy, University of Washington, Box 351580, Seattle, WA 98195-1580, USA
[3] Department of Physics, University of Notre Dame, 225 Nieuwland Science Hall, Notre Dame, IN 46556, USA
[4] Department of Astronomy, California Institute of Technology, 1200 E. California Blvd, Pasadena, CA 91125, USA
[5] Department of Physics and Astronomy, Vanderbilt University, Nashville, TN 37235, USA
[6] Observatório do Valongo, Universidade Federal do Rio de Janeiro, Ladeira do Pedro Antônio, 43, CEP: 20080-090, Rio de Janeiro, RJ, Brazil
[7] Laboratório Interinstitucional de e-Astronomia (LIneA), Rio de Janeiro, RJ 20921-400, Brazil
[8] Instituto de Astrofísica de Canarias, C/Vía Lctea S/N, E-38200 La Laguna, Spain
[9] Departamento de Astrofísica, Universidad de La Laguna, E-38205 La Laguna, Tenerife, Spain
[10] Department of Astronomy and Astrophysics, The Pennsylvania State University, 525 Davey Laboratory, University Park, PA 16802, USA
[11] Center for Exoplanets and Habitable Worlds, The Pennsylvania State University, University Park, PA 16802, USA
[12] Department of Astronomy, The Ohio State University, 140 West 18th Avenue, Columbus, OH 43210, USA
[13] Observatório Nacional, Rua General José Cristino 77, 20921-400 São Cristóvão, Rio de Janeiro, RJ, Brazil
[14] Department of Physics, Fisk University, 1000 17th Ave. N., Nashville, TN 37208, USA
[15] Homer L Dodge Department of Physics & Astronomy, University of Oklahoma, 440 W Brooks St, Norman, OK 73019, USA
[16] Apache Point Observatory, P.O. Box 59, Sunspot, NM 88349-0059, USA
[17] Las Cumbres Observatory Global Telescope Network, 6740 Cortona Drive, Suite 102, Santa Barbara, CA 93117, USA
[18] Department of Physics Broida Hall, University of California, Santa Barbara, CA 93106, USA
[19] NASA Exoplanet Science Institute, Caltech, MS 100-22, 770 South Wilson Avenue, Pasadena, CA 91125, USA
[20] Center for Cosmology and Particle Physics, New York University, New York, NY, USA
[21] Consejo Superior de Investigaciones Cientficas, Spain
[22] Instituto de Física, UFRGS, Caixa Postal 15051, Porto Alegre, RS 91501-970, Brazil
[23] Indian Institute of Astrophysics, II Block, Koramangala, Bangalore 560 034, India
[24] MIT Kavli Institute for Astrophysics & Space Research, Cambridge, MA 02139, USA
[25] Steward Observatory, University of Arizona, Tucson, AZ 85121, USA
[26] Department of Astronomy, MSC 4500, New Mexico State University, P.O. Box 30001, Las Cruces, NM 88003, USA
Received 2012 June 26; accepted 2012 November 2; published 2012 December 12

ABSTRACT

We present an eccentric, short-period brown dwarf candidate orbiting the active, slightly evolved subgiant star TYC 2087-00255-1, which has effective temperature $T_{\rm eff} = 5903 \pm 42$ K, surface gravity $\log(g) = 4.07 \pm 0.16$ (cgs), and metallicity $[{\rm Fe/H}] = -0.23 \pm 0.07$. This candidate was discovered using data from the first two years of the Multi-object APO Radial Velocity Exoplanets Large-area Survey, which is part of the third phase of Sloan Digital Sky Survey. From our 38 radial velocity measurements spread over a two-year time baseline, we derive a Keplerian orbital fit with semi-amplitude $K = 3.571 \pm 0.041$ km s^{-1}, period $P = 9.0090 \pm 0.0004$ days, and eccentricity $e = 0.226 \pm 0.011$. Adopting a mass of $1.16 \pm 0.11\ M_{\odot}$ for the subgiant host star, we infer that the companion has a minimum mass of $40.0 \pm 2.5\ M_{\rm Jup}$. Assuming an edge-on orbit, the semimajor axis is 0.090 ± 0.003 AU. The host star is photometrically variable at the ∼1% level with a period of $\sim 13.16 \pm 0.01$ days, indicating that the host star spin and companion orbit are not synchronized. Through adaptive optics imaging we also found a point source 643 ± 10 mas away from TYC 2087-00255-1, which would have a mass of $0.13\ M_{\odot}$ if it is physically associated with TYC 2087-00255-1 and has the same age. Future proper motion observation should be able to resolve if this tertiary object is physically associated with TYC 2087-00255-1 and make TYC 2087-00255-1 a triple body system. Core Ca II H and K line emission indicate that the host is chromospherically active, at a level that is consistent with the inferred spin period and measured $v_{\rm rot} \sin i$, but unusual for a subgiant of this $T_{\rm eff}$. This activity could be explained by ongoing tidal spin-up of the host star by the companion.

Key words: brown dwarfs – stars: low-mass – techniques: radial velocities

Online-only material: color figures

1. INTRODUCTION

Brown dwarfs (BDs) range in mass from ∼13 to 80 Jupiter masses and burn deuterium but not hydrogen (Burrows et al. 1997, 2001; Chabrier & Baraffe 2000; Spiegel et al. 2011). The first unambiguous discovery of BDs (Rebolo et al. 1995, 1996; Nakajima et al. 1995; Oppenheimer et al. 1995; Basri et al. 1996) occurred at the same time as the discovery of the first extra-solar

giant planet orbiting a main-sequence star (51 Peg b; Mayor & Queloz 1995). More than 800 BDs have been discovered to date (see DwarfArchives.org, http://www.dwarfarchives.org). Most of them are free-floating objects and only several dozen BDs are companions to other stars (Reid & Metchev 2008; Sahlmann et al. 2011). The BD desert (a paucity of BD companions relative to planetary or stellar companions within 3 AU around main-sequence FGKM stars) was found during high-precision radial velocity (RV) surveys seeking exoplanets (Marcy & Butler 2000). Since RV surveys are more sensitive to BDs than to exoplanets, this paucity is a real minimum in the mass distribution of close companions to solar-type stars. The California & Carnegie Planet Search finds a BD occurrence rate of 0.7% ± 0.2% from their sample of ∼1000 target stars (Vogt et al. 2002; Patel et al. 2007), and the McDonald Observatory Planet Search agrees with a rate of 0.8% ± 0.6% from a search sample of 250 stars (Wittenmyer et al. 2009). To assess the reality of the BD desert, Grether & Lineweaver (2006) performed a detailed investigation of the companions around nearby Sun-like stars. They find that approximately 16% of nearby Sun-like stars have close ($P < 5$ years) companions more massive than Jupiter: 11% ± 3% are stellar, <1% are BDs, and 5% ± 2% are giant planets. However, Gizis et al. (2001) suggest that BDs might not be as rare at wide separations (see also Metchev & Hillenbrand 2004). Lafrenière et al. (2007) obtain a 95% confidence interval of $1.9^{+8.3}_{-1.5}$% for the frequency of 13–75 $M_{\rm Jup}$ companions between 25 and 250 AU amongst 85 nearby young stars observed during the Gemini Deep Planet Survey. Based on an adaptive optics (AO) survey for substellar companions, Metchev & Hillenbrand (2009) infer that the frequency of BDs in 28–1590 AU orbits around young solar analogs is $3.2^{+3.1}_{-2.7}$%.

Ostensibly, BDs are believed to form similarly to stars, through gravitational collapse and/or fragmentation of molecular clouds (Padoan & Nordlund 2004; Hennebelle & Chabrier 2008). However, companions with masses up to 10 $M_{\rm Jup}$ (Alibert et al. 2005) or even 25 $M_{\rm Jup}$ (Mordasini et al. 2008) may form in protoplanetary disks. As such, the BD desert is commonly interpreted as the gap between the largest mass objects that can be formed in disks and the smallest mass clump that can collapse and/or fragment in the vicinity of a protostar. In comparison, the mass function of isolated substellar objects both in the field and in clusters appears to be roughly flat in $\log(M)$ for masses down to at least ∼20 $M_{\rm Jup}$ (Luhman et al. 2000; Chabrier 2002). Recently, André et al. (2012) found a self-gravitating condensation of gas and dust with a mass of 0.015–0.03 $M_{\odot}$ using millimeter interferometric observations, which supports the idea that BDs could form the same way as stars.

Given the occurrence rate of ∼1% for BD companions, a large, relatively uniform, systematic RV survey of a much larger sample of stars is needed to make further progress in understanding properties of the BD desert. The Multi-object APO Radial Velocity Exoplanets Large-area Survey (MARVELS; Ge et al. 2008) is a four-year RV survey of ∼3300 stars with $7.6 < V < 12$ over time baselines of ∼1.5 years per target, with a stated goal of <30 m s^{-1} precision for the faintest stars. MARVELS uses the innovative instrumental technique of a dispersed fixed-delay interferometer (DFDI; see, e.g., Erskine & Ge 2000; Ge 2002; Ge et al. 2009; van Eyken et al. 2010; Wang et al. 2011, 2012a, 2012b) in order to simultaneously observe 60 objects at a time. By virtue of the large number of target stars, as well as the addition of uniform selection criteria described in Lee et al. (2011), MARVELS is well suited to detect significant numbers of rare companions. For example, Lee et al. (2011) have recently announced MARVELS-1b, a 5.9 day BD candidate around the F-type star TYC 1240-00945-1 located in the BD desert.

This paper is part of a series that describes the very-low-mass stellar and substellar companions to solar-like stars detected in the MARVELS survey (Lee et al. 2011; Wisniewski et al. 2012; Fleming et al. 2012). In this paper, we report a new MARVELS BD candidate, which we designate MARVELS-4b, detected in orbit around the star TYC 2087-00255-1 (*Tycho-2* star catalog; Høg et al. 2000). In Section 2 we describe the observations used in this paper. We present stellar parameters for the star in Section 3 and orbital parameters for the BD candidate in Section 4. We discuss these results and give our conclusions in Section 5.

2. OBSERVATIONS AND PROCESSING

2.1. MARVELS Radial Velocities

TYC 2087-00255-1 was a target in the first two-year cycle of the SDSS-III (Eisenstein et al. 2011) MARVELS planet search program. This star was selected for RV monitoring using the preselection methodology and instrumentation described in Lee et al. (2011). The RV observations were taken using the Sloan Digital Sky Survey (SDSS) 2.5 m telescope at Apache Point Observatory (Gunn et al. 2006) coupled to the MARVELS instrument (Ge et al. 2009), a 60 object, fiber-fed, DFDI. The interferometer produces two fringing spectra ("beams") per object, in the wavelength range ∼500–570 nm, with resolving power $R \sim 12{,}000$. TYC 2087-00255-1 was observed at 23 epochs from 2009 May 4 to 2010 July 5. Lee et al. (2011) describe the basic data reduction and analysis leading to the production of differential RVs. The RV errors are scaled by a "quality factor" $Q = 6.22$ based on the rms errors of the other stars observed on the same SDSS-III plate as TYC 2087-00255-1 (Fleming et al. 2010). The differential RV measurements for TYC 2087-00255-1 from MARVELS are summarized in Table 1. Note that a constant velocity term has been subtracted to account for the instrument offset (see Section 4.1 for more detail).

2.2. Spectra for Stellar Characterization

In pursuit of precise stellar parameters for the primary, optical (∼3500–9000 Å) spectra of TYC 2087-00255-1 were obtained using the FEROS high-resolution ($R = 48{,}000$) spectrograph (Kaufer et al. 1999) mounted on the MPG/ESO 2.2 m telescope in La Silla on 2010 August 2. FEROS spectra were analyzed using the online FEROS Data Reduction System and the standard calibration plan, where bias, flat-field, and wavelength calibration lamp frames are observed in the afternoon. Three 2400 s exposures were combined to yield a signal-to-noise ratio (S/N) of ∼230 per one-dimensional extracted pixel at 6600 Å.

Additional spectroscopic observations around the Hα line were also secured with the coudé spectrograph of the 1.60 m telescope at Observatório do Pico dos Dias, Brazil on 2010 August 17. The resolution was set to $R = 18{,}000$ and the S/N per pixel was ∼80. Data reduction was carried out by the standard procedure using IRAF. After usual bias and flat-field correction, we subtracted the background and scattered light and extracted one-dimensional spectra. No fringing was present in our spectra. The Observatório do Pico dos Dias (OPD) coudé single-order spectrograph introduces no necessity for blaze function corrections and thus the line profile is easily

Table 1
Summary of Marvels Radial Velocities

HJD	RV (km s^{-1})	σ_{RV} (km s^{-1})
2454955.86681	−1.728	0.056
2454995.81378	3.007	0.048
2455020.70639	−3.583	0.045
2455025.65578	2.354	0.053
2455106.66179	2.333	0.053
2455107.63962	1.155	0.053
2455255.00502	−3.105	0.094
2455259.00872	3.111	0.045
2455281.89957	−3.211	0.063
2455284.87791	3.465	0.059
2455286.89844	2.444	0.051
2455291.86506	−0.911	0.053
2455292.87266	2.390	0.057
2455311.89105	3.574	0.053
2455312.80083	3.190	0.061
2455314.80872	1.226	0.055
2455338.78513	3.564	0.044
2455346.71409	1.869	0.095
2455347.70953	3.507	0.072
2455350.83978	0.905	0.067
2455374.88651	3.536	0.052
2455381.88436	−1.373	0.061
2455382.91902	2.255	0.065

normalized, lending itself to accurate analysis of the temperature profile of the stellar atmosphere by fitting the observed profile to theoretical calculations. This will be used below to infer an independent $T_{\rm eff}$ estimate as well as the evaluation of the chromospheric radiative losses in the Hα line core.

2.3. Additional Radial Velocity Observations

High-resolution spectra were collected with the Spectrografo di Alta Resoluzione Galileo (SARG) spectrograph (Gratton et al. 2001) at the 3.58 m Telescopio Nazionale Galileo (TNG) for additional RV measurements from 2010 August 27 to 2011 August 17. This spectrograph provides $R \sim 57{,}000$ spectra spanning a wavelength range of 462–792 nm. The spectra were reduced using standard IRAF Echelle reduction packages. Frames were trimmed, bias subtracted, flat-field corrected, aperture-traced, and extracted. We obtained 15 epochs of observations with an iodine cell and an additional epoch without the iodine cell to serve as a stellar template. The exposure time for each epoch is 20–30 minutes. The S/N per resolution element at 550 nm is ∼60–250, and one resolution element is sampled by 4.9 pixels. A total of 15 RV data points were derived using the iodine cell technique (Marcy & Butler 2000). Each of 21 SARG orders between 504 and 611 nm was subdivided into 10 sections, and then RVs were measured from these components. Following a 2σ clip, the measurements were averaged to produce the RVs. The resultant differential RVs are summarized in Table 2. Note that a constant velocity term has been subtracted to account for the instrument offset (see Section 4.1).

2.4. Diffraction-limited Imaging

High angular resolution lucky images (LIs, observations taken at very high cadence to achieve nearly diffraction-limited images from a subsample of the total) were obtained using FastCam (Oscoz et al. 2008) on the 1.5 m TCS telescope at Observatorio

Table 2
Summary of SARG Radial Velocities

HJD	RV (km s^{-1})	σ_{RV} (km s^{-1})
2455436.40537	0.679	0.046
2455436.49082	0.960	0.066
2455460.36043	−1.475	0.019
2455460.38315	−1.493	0.018
2455495.32045	0.467	0.068
2455495.33502	0.318	0.096
2455495.35302	0.259	0.137
2455666.65770	0.096	0.044
2455698.58443	3.028	0.010
2455725.45470	2.654	0.022
2455725.48125	2.701	0.020
2455725.53485	2.801	0.021
2455760.43524	−0.550	0.035
2455760.56766	0.133	0.044
2455791.50436	2.219	0.032

del Teide, Spain. The primary goal of these observations was to search for companions at large separations that could pollute spectroscopic RV observations of the targets. The LI frames were acquired on 2011 May 8 and 2011 July 1 in the *I* band, covering ∼21″ × 21″ on the sky. A total of 60,000 images, each corresponding to 60 ms integrations, were taken on 2011 May 8, and a total of 64,000 frames, each corresponding to 50 ms integrations, were taken on 2011 July 1.

To further assess the multiplicity of TYC 2087-00255-1, we acquired AO images using NIRC2 (instrument built by Keith Matthews) on the Keck II telescope on 2012 August 25 UT. TYC 2087-00255-1 is bright ($V = 10.6$) and served as its own on-axis natural guide star. NIRC2 is a high-resolution near-infrared camera that provides a plate scale (when operating in narrow mode) of 9.963 ± 0.006 mas pixel^{-1} (Ghez et al. 2008) and 10.″2 × 10.″2 field of view. Our observations consist of dithered frames taken with the *K*-band ($\lambda_c = 2.12$ μm, $\Delta\lambda = 0.35$ μm) filter. The total on-source integration time was 47.5 s.

2.5. SuperWASP Photometric Data

To check for intrinsic photometric variability indicating stellar activity and search for possible transits of the companion, we extracted photometric time series data of TYC 2087-00255-1 from the SuperWASP public archive (Butters et al. 2010). The WASP instruments provide flux measurements for millions of stars using wide-angle images of the night sky over a bandpass of 400–700 nm defined by a broadband filter. Eight cameras on each instrument provide images covering approximately 7.°8 × 7.°8 using Canon 200 mm *f*/1.8 camera lenses and e2v 2048 × 2048 CCDs. Synthetic aperture photometry using an aperture radius of 49 arcsec at the position of targeted stars is performed on the images (Pollacco et al. 2006). A total of 18,935 aperture photometry data points, each taken with a 30 s integration time, were available from the SuperWASP public archive. These data were taken between 2004 May 2 and 2008 August 10. Systematic errors caused by spatially localized flat-fielding, errors in the vignetting correction near the edge of the field of view, bright moonlight contamination, bad weather, and other as-yet-unidentified reasons do exist in SuperWASP data sets (Collier Cameron et al. 2006). There are large systematic errors in some of the data sets, and we choose to use data points with relative flux errors smaller than 0.01 in our further analysis,

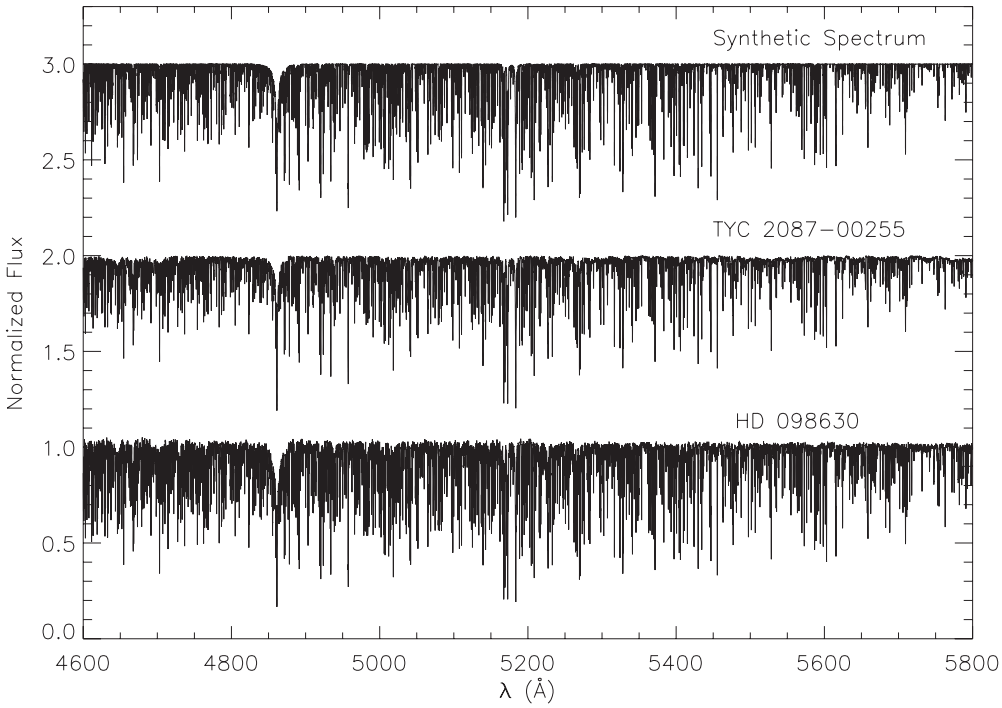

Figure 1. Continuum-normalized, high-resolution FEROS spectra of TYC 2087-00255-1, which is a G0IV star. For comparison purpose, also shown in this plot are the spectrum of a G0IV star HD 098630 from Elodie spectra library (Prugniel & Soubiran 2001) and the synthetic spectrum of TYC 2087-00255-1 calculated using SME package (please see the text for more information). The FEROS spectrum and the synthetic spectrum have been shifted in the *y*-axis direction for display purpose.

Table 3
Spectroscopic Parameters of the Star TYC 2087-00255-1

$T_{\rm eff}$ (K)	log(g) (cgs)	[Fe/H]	ξ_t (km s^{-1})	Notes
5805 ± 71	4.02 ± 0.18	-0.24 ± 0.10	1.74 ± 0.10	BPG (ESO 2.2 m)
5941 ± 44	4.15 ± 0.22	-0.23 ± 0.08	1.687 ± 0.055	IAC (ESO 2.2 m)
5903 ± 42	4.07 ± 0.16	-0.23 ± 0.07	1.70 ± 0.06	Combined results

to limit systematics. The final selected data sets have a total of 11,932 photometric data points.

3. TYC 2087-00255-1: THE STAR

3.1. Stellar Parameters

We have used two independent pipelines (referred to as "BPG" and "IAC") to derive the stellar parameters from the high-resolution FEROS spectra. Both methods involve analysis of the equivalent widths of Fe I and Fe II lines to balance the excitation and ionization equilibria of these features. These two methods are described in detail in Wisniewski et al. (2012). Both pipelines produce values of effective temperature $T_{\rm eff}$, surface gravity log(g), and metallicity [Fe/H] mutually consistent. Because both pipeline determinations are mutually consistent, we average these two sets weighted by their own pipeline errors to determine the final stellar parameters, shown as "combined results" in Table 3. For each stellar parameter, we add in quadrature a systematic error of 18 K, 0.08 and 0.03 for $T_{\rm eff}$, log(g) and [Fe/H], respectively, in addition to the internal errors inherent from the two pipeline results (see Wisniewski et al. 2012). The results are summarized in Table 3. The adopted stellar parameters are $T_{\rm eff} = 5903 \pm 42$ K, log(g) $= 4.07 \pm 0.16$ (cgs), and [Fe/H] $= -0.23 \pm 0.07$. So TYC 2875-00255-1 is a G0IV type star. In Figure 1 we show the continuum-normalized high-resolution FEROS spectra of TYC 2087-00255-1 together with the spectra of HD 098630, a known G0IV type star from Elodie spectra library (Prugniel & Soubiran 2001). For comparison purpose, we also show synthetic spectra of TYC 2087-00255-1 in Figure 1. The synthetic spectra are calculated using software package Spectroscopy Made Easy (SME; Valenti & Piskunov 1996) and the stellar parameters from the above analysis.

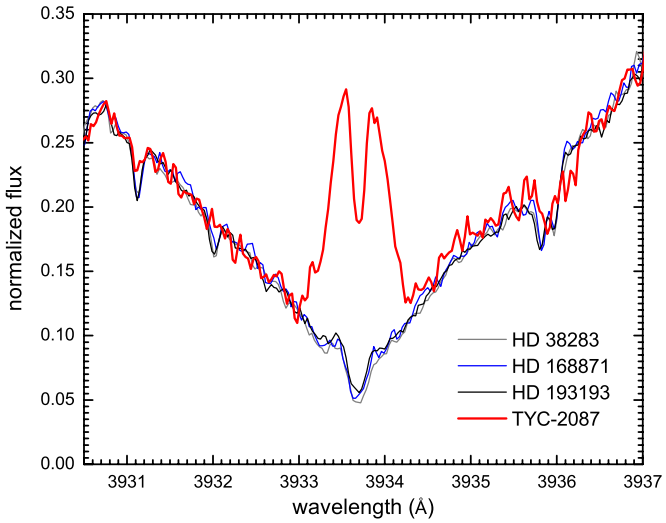

Figure 2. Continuum-normalized, high-resolution FEROS spectra of TYC 2087-00255-1 centered on the Ca II K line. The excess emission from the Ca II K line core indicates that TYC 2087-00255-1 is a chromospherically active star. Also shown on this plot are several chromospherically quite stars with similar stellar parameters to TYC 2087-00255-1 for comparison purpose (Ghezzi et al. 2010a, 2010b).

Continuum-normalized, high-resolution FEROS spectra of TYC 2087-00255-1 centered on the Ca II K line are shown in Figure 2. Also shown in this plot are three stars with similar stellar parameters as TYC 2087-00255-1 (Ghezzi et al.

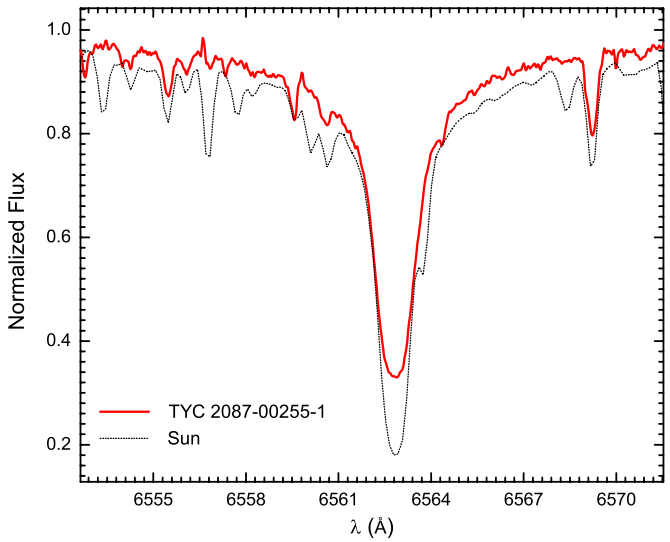

Figure 3. Continuum-normalized Hα profile of TYC 2087-00255-1, with a spectroscopic resolution of 18,000. Also shown on the plot is Hα profile of the Sun for comparison. The solar spectrum is measured from the reflected light of the Sun by Ganymede, taken together with TYC 2087-00255-1 using the same instrument. The shallower wing profile and the stronger core filling in the Hα line when compared to the Sun suggests an effective temperature lower than the spectroscopic temperature, which is also found by the SED analysis.

(A color version of this figure is available in the online journal.)

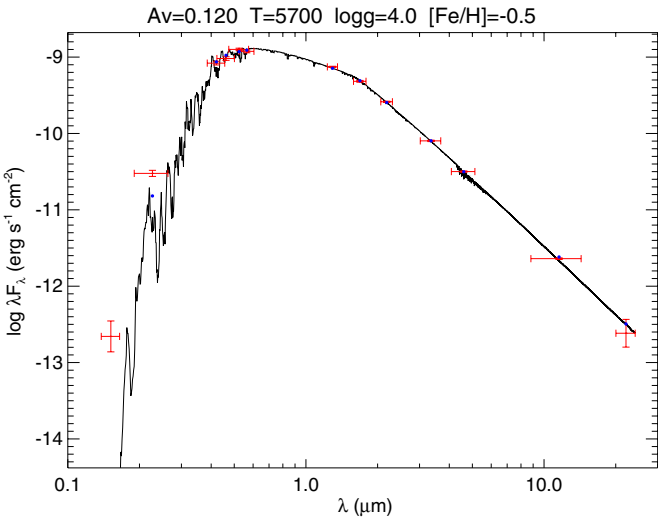

Figure 4. Observed SED from the near-UV through the IR for TYC 2087-00255-1, along with a best-fit NextGen model atmosphere. Blue points represent the expected fluxes in each band based on the model, red horizontal bars are the approximate bandpass widths, and red vertical bars are the flux uncertainties. There is potentially some *GALEX* FUV excess indicating this star is chromospheric active. The resultant fundamental stellar parameters from this fit agree with the stellar parameters determined from the stellar spectra to within 1σ.

(A color version of this figure is available in the online journal.)

Table 4
Photometric Measurements of the Star TYC 2087-00255-1

Parameter	Value	Note
$galFUV$	21.285 ± 0.506	*GALEX* (Morrissey et al. 2007)
$galNUV$	15.511 ± 0.013	*GALEX* (Morrissey et al. 2007)
B	11.203 ± 0.059	Kharchenko & Roeser (2009)
BT	11.32 ± 0.06	Høg et al. (2000)
V	10.553 ± 0.048	Kharchenko & Roeser (2009)
VT	10.58 ± 0.04	Høg et al. (2000)
$J2M$	9.29 ± 0.02	Cutri et al. (2003)
$H2M$	8.96 ± 0.03	Cutri et al. (2003)
$K2M$	8.88 ± 0.02	Cutri et al. (2003)
$WISE1$	8.839 ± 0.024	Cutri et al. (2012)
$WISE2$	8.864 ± 0.022	Cutri et al. (2012)
$WISE3$	8.792 ± 0.027	Cutri et al. (2012)
$WISE4$	9.169 ± 0.454	Cutri et al. (2012)

2010a, 2010b). The excess emission from the Ca II K line core indicates that TYC 2087-00255-1 is more active than stars with similar stellar parameters. Using the high-resolution FEROS spectra and the method described in Jenkins et al. (2008), the chromospheric Ca II HK activity index of TYC 2087-00255-1 is $\log R'_{\rm HK} = -4.58$, with a calibration rms error of 0.03.

The Hα profile of TYC 2087-00255-1 is shown in Figure 3 superimposed over the solar one, the latter obtained as a disk-integrated spectrum from Ganymede (which reflects light from the Sun) under the same observational conditions. The shallower wing profile is apparent, translating into a lower $T_{\rm eff}$ for TYC 2087-00255-1, as is the much stronger line core filling, interpreted as additional chromospheric fill-in. Note that the Hα line core is substantially broader in TYC 2087-00255-1, interpreted as yet another confirmation of the subgiant status of TYC 2087-00255-1 (Pasquini & Pallavicini 1991; Lyra & Porto de Mello 2005). The chromospheric loss in the Hα core of TYC 2087-00255-1 was also evaluated under the prescription of Lyra & Porto de Mello (2005), using as input the spectroscopic atmospheric parameters. We have derived a total chromospheric flux of 13.4×10^5 erg cm^{-2} s^{-1} inside the Hα line core, the estimated error in the Lyra & Porto de Mello (2005) procedure being $\sim 0.5 \times 10^5$ erg cm^{-2} s^{-1}. This value is probably also contaminated by veiling from the companion, and should be taken as an upper limit. Nonetheless, it is over four times the expected flux from typical subgiants in this $T_{\rm eff}$ range (Figure 3 of Lyra & Porto de Mello 2005) and lies between the average chromospheric radiative losses of Pleiades (age ~100 Myr) and Ursa Major group stars (~400 Myr). This flux is in very good agreement with the Ca II K line profile (which being in the UV is probably free from the secondary's contamination) in pointing to a very high activity level in TYC 2087-00255-1, compatible with a solar-type stars no more than a few hundred million years of age (Lyra & Porto de Mello 2005). Two independent spectroscopic chromospheric indicators therefore confirm TYC 2087-00255-1 as much more active than expected from its subgiant status.

The spectral energy distribution (SED) was constructed for TYC 2087-00255-1 in Figure 4 using near-UV (*GALEX*; Morrissey et al. 2007), optical (Høg et al. 2000; Kharchenko & Roeser 2009), near-IR (2MASS, Cutri et al. 2003), and IR (*WISE*; Wright et al. 2010; Cutri et al. 2012) photometric data. These photometric data are presented in Table 4. The data were fit with fluxes from a NextGen model atmosphere (Hauschildt et al. 1999). We limited the maximum line-of-sight extinction to be $A_V < 0.15$ based on the analysis of dust maps by Schlegel et al. (1998). The resultant parameters, $T_{\rm eff} = 5700 \pm 200$ K, $\log(g) = 4.0 \pm 0.5$, [Fe/H] $= -0.5 \pm 0.5$, and $A_V = 0.12^{+0.03}_{-0.06}$, agree within 1σ of the results found via analysis of our high-resolution spectroscopy. In the above analysis, we did not constrain any of the fit parameters except for A_V. We did another fit where we forced $T_{\rm eff}$, $\log(g)$ and [Fe/H] to the spectroscopically determined values, which provide a more robust estimate of $A_V = 0.12 \pm 0.03$. Using this total extinction

Table 5
Derived Parameters of the Star TYC 2087-00255-1

Parameter	Value
Spectral type	G0 IV
Mass	$1.16 \pm 0.11\ M_{\odot}$
Radius	$1.64 \pm 0.37\ R_{\odot}$
Age	5.5 Gyr
A_V	$0.12^{+0.03}_{-0.06}$
Distance	218 ± 14 pc
$\log R'_{\rm HK}$	−4.58

estimate, and adopting a V-band bolometric correction BC_V of -0.19 ± 0.02 (Cox 2000), we estimate that the distance to this system is 218 ± 14 pc.

3.2. Stellar Mass and Radius

We determine the mass and radius of the parent star, TYC 2087-00255-1, from $T_{\rm eff}$, $\log(g)$, and [Fe/H] using the empirical polynomial relations of Torres et al. (2010), which were derived from a sample of eclipsing binaries with precisely measured masses and radii. We estimate the uncertainties in M_* and R_* by propagating the uncertainties in $T_{\rm eff}$, $\log(g)$, and [Fe/H] (see Table 5) using the covariance matrices of the Torres et al. (2010) relations (kindly provided by G. Torres). Since the polynomial relations of Torres et al. (2010) were derived empirically, the relations were subject to some intrinsic scatter, which we add in quadrature to the uncertainties propagated from the stellar parameter measurements ($\sigma_{\log m} = 0.027$ and $\sigma_{\log r} = 0.014$; Torres et al. 2010). The final stellar mass and radius values obtained are $M_* = 1.16 \pm 0.11\ M_{\odot}$ and $R_* = 1.64 \pm 0.37\ R_{\odot}$ (see Table 5).

3.3. Evolutionary State

In Figure 5 we compare the spectroscopically measured $T_{\rm eff}$ and $\log(g)$ of TYC 2087-00255-1 (red error bars) against a theoretical stellar evolutionary track from the Yonsei–Yale ("Y^2") model grid (Demarque et al. 2004). The solid curve represents the evolution of a single star of mass $1.16 \pm 0.11\ M_{\odot}$ and metallicity of [Fe/H] $= -0.23 \pm 0.07$. The dashed curves represent the same evolutionary track but for masses $\pm 0.08\ M_{\odot}$, which represents the 1σ uncertainty in our derived mass. The filled gray region between the mass tracks represents the expected location of a star of TYC 2087-00255-1's mass and metallicity as it evolves off the main sequence. The spectroscopically measured $T_{\rm eff}$, $\log(g)$, and [Fe/H] place TYC 2087-00255-1 in the subgiant phase, prior to the base of the red giant branch, with an estimated age of ∼5.5 Gyr.

3.4. Stellar Rotation Period and Rotational Velocity

In this section, we will use three different ways to estimate the rotation period of TYC 2087-00255-1. First, we find a sinusoidal variation in the 2004 SuperWASP photometry data with a period $P = 13.16 \pm 0.01$ days and amplitude of 9 mmag. In Figure 6 we have shown a phase-folded plot of the 2004 SuperWASP data. Since the SuperWASP photometry data used an aperture radius of 49 arcsec, we used the SIMBAD Web site to check for bright stars inside this 49 arcsec aperture which could account for this 9 mmag variation and found several stars with $V_{\rm mag} > 16.2$. Such faint stars could not produce such a 9 mmag variation around the $V_{\rm mag} = 10.6$ TYC 2087-00255-1 unless their luminosities varied by 100%, which is quite unlikely. We can explain this 13.16 day period as the rotation period of the host star and the 9 mmag sinusoidal variation by the rotational modulation of starspots.

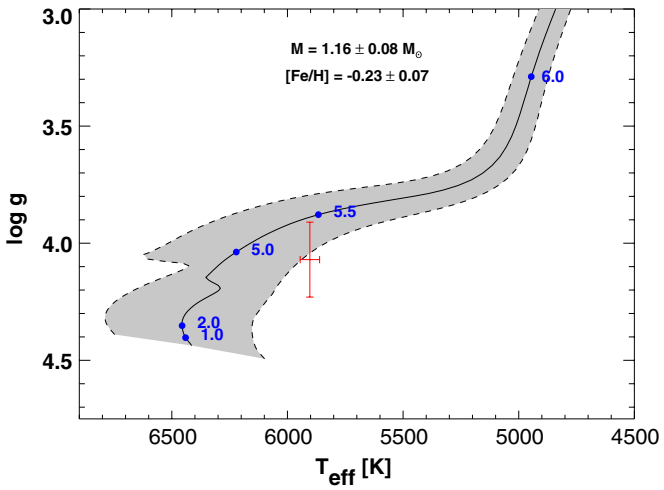

Figure 5. Evolutionary track for an object with $M = 1.16\ M_{\odot}$, at [Fe/H] $= -0.23$. Ages of 1, 2, 5, 5.5, and 6 Gyr are indicated as dots. The possible tracks for $\pm 1\sigma$ deviation in the mass are shown by the shaded region. The stellar parameters for TYC 2087-00255-1, with 1σ error bars, are shown by the cross. (A color version of this figure is available in the online journal.)

The second method to derive the rotation period is to use the chromospheric activity–rotation relation (Mamajek & Hillenbrand 2008). The chromospheric Ca II HK activity index of TYC 2087-00255-1 derived previously is $\log R'_{\rm HK} = -4.58$. The corresponding rotation period is 11.8 days, with an estimated error of 2.4 days from this calibrated relation. This rotation period agrees with the one derived above (13.16 days) using the SuperWASP photometry data. However, we should note here that this chromospheric activity–rotation relation is derived for solar-type dwarf stars. Since TYC 2087-00255-1 is a slightly evolved subgiant, it may not be appropriate to use this relation here.

Third, we use the equation $2\pi R_*/v_{\rm rot} \sin i$ to estimate the rotation period of the host star. We measured the projected rotational velocity $v_{\rm rot} \sin i$ of TYC 2087-00255-1 by comparing our high-resolution SARG and FEROS spectrum to broadened versions of Kurucz ATLAS synthetic spectra. We used the atmospheric parameters derived in Section 3.1 and fixed the macro turbulence velocity to $V_{\rm macro} = 4.2$ km s^{-1} based on Equation (1) from Valenti & Fischer (2005). We find $v_{\rm rot} \sin i = 9.2 \pm 2.0$ km s^{-1} using the observed SARG spectrum and $v_{\rm rot} \sin i = 10.1 \pm 0.9$ km s^{-1} using the observed FEROS spectrum. Using the derived radius of TYC 2087-00255-1 $R_* = 1.64 \pm 0.37\ R_{\odot}$, the corresponding rotation period are 9.1 ± 2.9 days and 8.3 ± 2.0 days. These are about 1.4σ and 2.4σ from the 13.16 day period inferred from photometric data, suggesting that the star is likely close to edge-on, as a smaller inclination would imply shorter periods and thus larger discrepancy with the photometric period. The slight tension even assuming $\sin i = 1$ may arise from systematic errors in the estimate of $v_{\rm rot} \sin i$, including an incorrect assumed value for $V_{\rm macro}$.

4. TYC 2087-00255-1: THE COMPANION

4.1. Keplerian Orbital Solution

RVs derived from MARVELS and SARG data were used to fit Keplerian orbital parameters. Since there are starspot

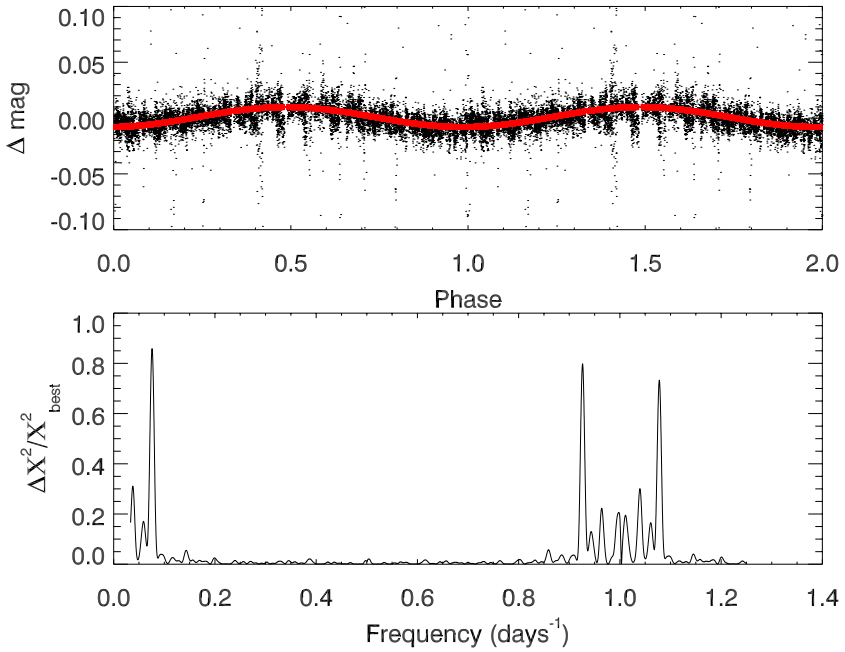

Figure 6. Top: phase-folded light curve for TYC 2087-00255-1 at a period of 13.16 day from SuperWASP. Bottom: Lomb–Scargle periodogram of the SuperWASP data, showing no evidence for any significant periodicities around $P = 9$ days (frequency of 0.11 day^{-1}, the orbital period of MARVELS-4b). Instead there is evidence of a significant period at 13.16 days (frequency of 0.076 day^{-1}), which is likely the rotational period of TYC 2087-00255-1 as tracked by rotational modulation of starspots. There are several peaks around the one-day period, which are daily aliases.

(A color version of this figure is available in the online journal.)

Table 6
MARVELS-4b: Parameters of the Companion

Parameter	MARVELS+TNG	MARVELS
Minimum mass	$40.0 \pm 2.5\ M_{\rm Jup}$	$39.9 \pm 2.5\ M_{\rm Jup}$
a	0.090 ± 0.003 AU	0.090 ± 0.003 AU
K (km s^{-1})	3.571 ± 0.041 km s^{-1}	3.563 ± 0.073 km s^{-1}
P (days)	9.0090 ± 0.0004 days	9.0105 ± 0.0024 days
e	0.226 ± 0.011	0.233 ± 0.022
w	4.086 ± 0.041	4.077 ± 0.081
$\sigma_{\rm jitter}$	0.112 ± 0.017 km s^{-1}	0.152 ± 0.046 km s^{-1}
$T_{\rm prediction\ for\ transit}$ (HJD$_{\rm UTC}$)	2455549.629 ± 0.056	2455549.715 ± 0.082
$T_{\rm periastron}$ (HJD$_{\rm UTC}$)	2455552.797 ± 0.083	2455552.851 ± 0.147

features seen from the light curve of TYC 2087-00255-1 (see Section 3.4), we added an additional stellar "jitter" term ($\sigma_{\rm jitter}$) in our Keplerian orbital model as suggested by Ford (2006) to account for any additional noise induced by the stellar activity. We performed two Keplerian orbital fits using the Markov Chain Monte Carlo method (see, e.g., Ford 2006). First, we use only the MARVELS data to fit the Keplerian orbit, then we combine the MARVELS and SARG RV data to do a joint fit. For the details of our one planet/BD RV model, please see Section 2 of Gregory (2007). The best-fit parameters from the two fits are presented in Table 6 and they agree with each other quite well.

As expected, the fit of the combined MARVELS and SARG RV data has relatively smaller uncertainties compared to the fit with just the MARVELS data, therefore we use this combined fit as our final Keplerian orbital solution. In this fit, a constant systematic velocity term is included for each of the two instruments to account for the offset between the observed differential RV data and the zero point of the Keplerian RV model (-0.803 ± 0.035 km s^{-1} for MARVELS and -353 ± 0.029 km s^{-1} for SARG). The RV data shown in Table 1 and Table 2 are the RVs after subtraction of these two constant systematic velocity terms. The final Keplerian orbit of MARVELS-4b has a period $P = 9.0090 \pm 0.0004$ days, $e = 0.226 \pm 0.011$, and semi-amplitude $K = 3.571 \pm 0.041$ km s^{-1}. This solution is shown in Figures 7 and 8 together with the MARVELS and SARG RV data. The residuals shown in these two plots could not be explained only by the errors in our RV data. A stellar jitter term $\sigma_{\rm jitter} = 112 \pm 17$ m s^{-1} is required in our fitting to explain these residuals. In our previous paper (Fleming et al. 2010; Lee et al. 2011; Wisniewski et al. 2012), we did not include a stellar "jitter" term in our Keplerian fitting. Instead we rescaled the error bar of MARVELS RV data to force the reduced chi-square to be 1. Since MARVELS-4b is orbiting an active star which has spots activity, we choose to include this "jitter" term and did not try to rescale the MARVELS and SARG RV error bar. We note here that both methods (including a "jitter" term or rescaling the RV error bar for the reduced chi-square to be 1) yield Keplerian orbital parameters consistent with each other in the 1σ range. We will discuss more about this stellar jitter in Section 5.3. Using the derived value of M_* in Section 3.2, we estimate a minimum mass (i.e., for $\sin\alpha = 1$ where α is the line-of-sight orbital inclination) for the companion, MARVELS-4b, as $m_{\rm min} = 40.0 \pm 2.5\ M_{\rm Jup}$, where the uncertainty is dominated by the uncertainty in the primary

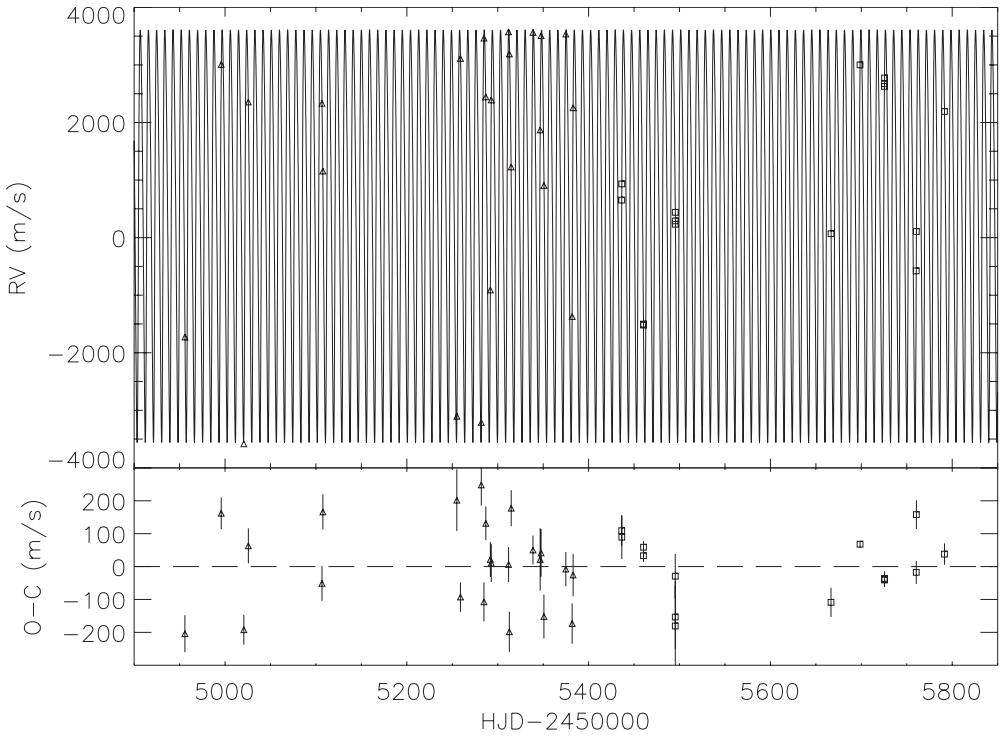

Figure 7. Top: Keplerian orbital solution for TYC 2087-00255-1. Open triangles are MARVELS discovery data, open squares are TNG data. Bottom: the residuals between the data points and the orbital solution.

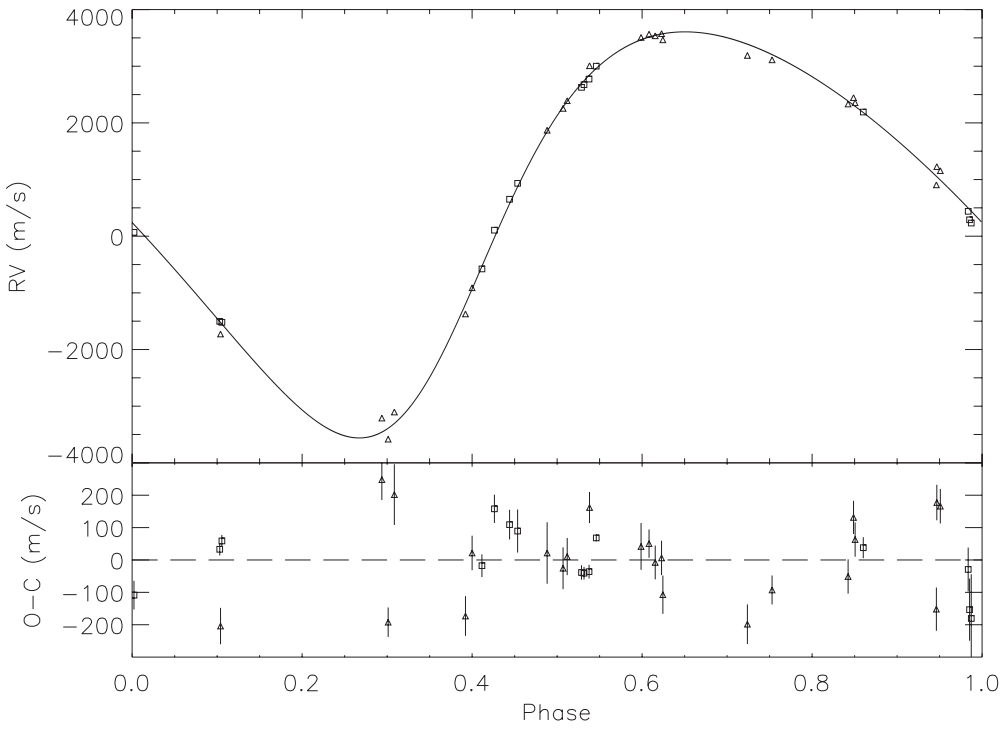

Figure 8. Top: phase-folded Keplerian orbital solution and RV residuals for TYC 2087-00255-1. Open triangles are MARVELS discovery data, open squares are TNG data. Bottom: the residuals between the data points and the orbital solution.

mass. Assuming the system to be edge-on, the semimajor axis of this system is $a = 0.090 \pm 0.003$ AU.

4.2. Search for Possible Transit Signals

Based on the orbital parameters of the companion, we have calculated the a priori transit probability to be 7.8% using Equation (5) from Kane & von Braun (2008). The expected duration of a central transit is $\sim R_* P/(\pi a) = 2.94$ hr, and the expected depth is $\sim (R/R_*)^2 = 0.004(R/R_{\rm Jup})^2$, where R is the radius of the companion. We phase folded the SuperWASP data and searched for a transit signal at the expected transit time, but no evidence for a transit with a period ~9 days was found. We could rule out existence of a transit signal with depth greater than

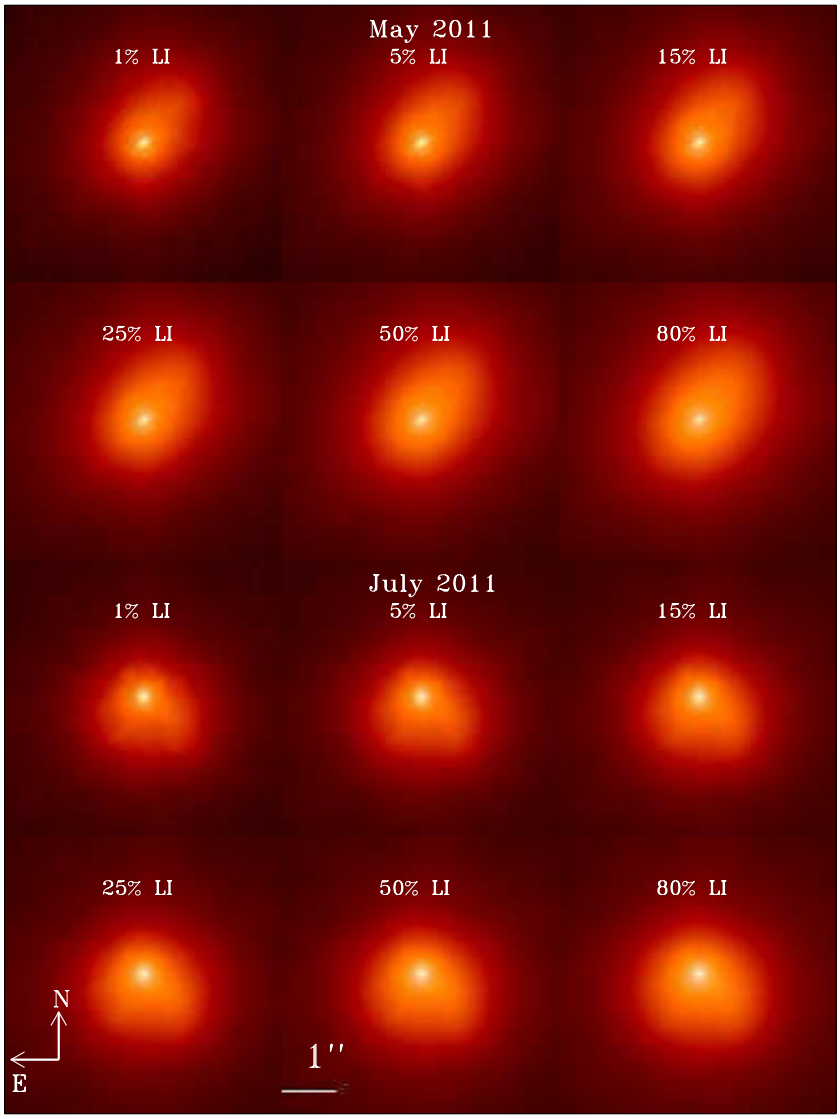

Figure 9. Composite images showing the results of different LI thresholds applied to frames acquired with FastCam on 2011 May 8 and 2011 July 1. Each panel covers ~5.5 × 5.5 arcsec^2, centered on TYC 2087-00255-1. To ease visualization, each image has been normalized to a peak value of unity. This set of images illustrates the gain in angular resolution close to the target location when applying highly restrictive LI thresholds, but at the cost of lowering the contrast achieved at larger angular distances from target location.

(A color version of this figure is available in the online journal.)

0.014 mag at the 3σ confidence level. Our conclusion is that the SuperWASP data are not sensitive enough to detect a 4 mmag transit signal. Further photometric follow-up observations are needed to rule out or confirm this transit signal.

4.3. Search for Possible Stellar Companions Using Lucky Imaging

We use the LIs to search for, and place constraints on, any possible undetected stellar companions at large separations. The data were processed using a custom IDL software pipeline. After identifying corrupted frames due to cosmic rays, electronic glitches, etc., the remaining frames are bias corrected and flat fielded. LI selection is applied using a variety of selection thresholds (best X%) based on the brightest pixel (BP) method. The selected BP must be below a specified brightness threshold to avoid selecting cosmic rays or other non-speckle features. As a further check, the BP must be consistent with the expected energy distribution from a diffraction speckle under the assumption of a diffraction-limited point-spread function. The frames are sorted from brightest to faintest according to the brightness of their BPs and the brightest X% are then shifted and added to generate a final image. In the different panels of Figure 9, we show the composite LIs generated from considering only the best {1, 5, 15, 25, 50, 80}% of the image frames. Each panel covers ~5.5 × 5.5 arcsec^2 centered on TYC 2087-00255-1. Restricting the images used to the best 1% improves the angular resolution with respect to the loose LI selection (i.e., the top 80% of the images image), but at the cost of increased noise at larger separations from the target. Following the same procedure as in Femenía et al. (2011), we compute the 3σ "best LI detectability curves" for each of the two nights' data, which are shown in the left panel of Figure 10. We use the following procedure to place a 3σ upper limit on the mass of a possible undetected stellar companion.

1. From the SED fitting of TYC 2087-00255-1 in Section 3.1 that provides an estimate of the extinction and distance,

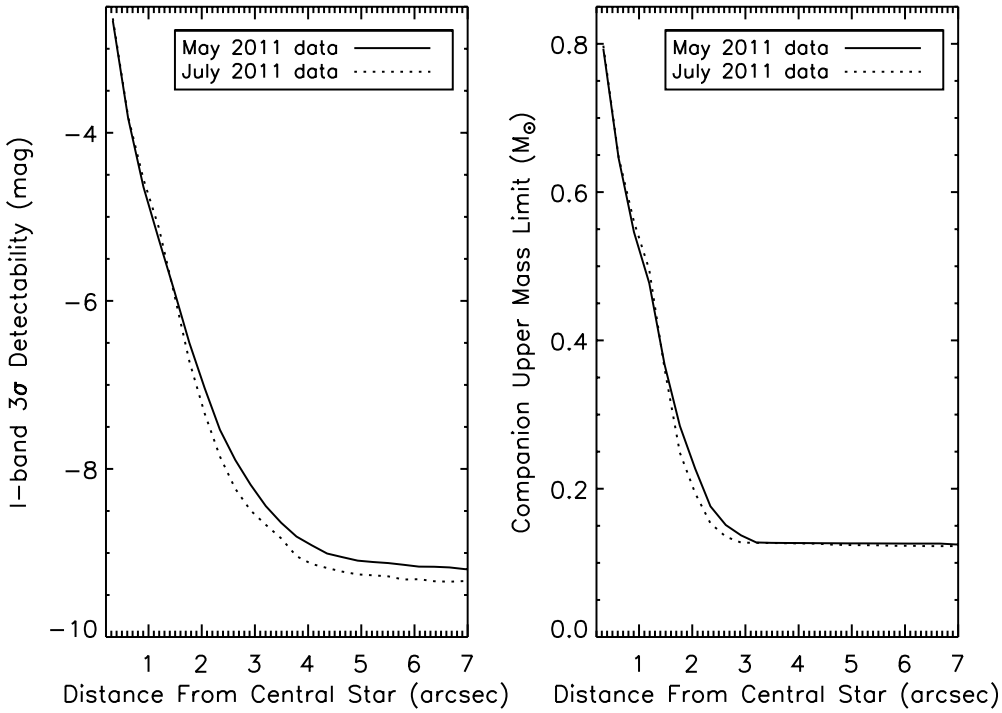

Figure 10. Left: best 3σ I-band detectability curves from lucky images achieved on 2011 July 1 and 2011 May 8. We see the quality of both nights is comparable. Right: conversion of 3σ detectability curves into mass sensitivities using empirical mass–luminosity relationships in the literature. See the main text for details.

we estimate the absolute I-band magnitude of TYC 2087-00255-1 to be $M_I = 2.74$.

2. Knowing M_I and the 3σ detectability curves (see the left panel of Figure 10) allows us to construct the M_I versus ρ (angular distance from TYC 2087-00255-1) curve for TYC 2087-00255-1. This curve provides the upper limit of absolute I-band magnitude for any undetected stellar companion at the 3σ level.
3. Although TYC 2087-00255-1 is identified as a subgiant, the fact that it is not very massive makes it plausible that any stellar companion with the same age and smaller mass will still be a main-sequence object. These facts justify the use of the conversion from I to V band in Mamajek (2010).
4. From the M_V versus ρ curves we employ the empirical mass–luminosity relationships from the literature (Henry et al. 1999; Delfosse et al. 2000; Henry 2004; Xia et al. 2008; Xia & Fu 2010) to derive the 3σ upper mass limit for any undetected companion as a function of angular distance to TYC 2087-00255-1.

The results of applying the above procedure to our LI data are shown in the right panel of Figure 10.

4.4. Search for Possible Stellar Companions Using AO Imaging

In this section we use the acquired Keck AO images to search for possible stellar companions around TYC 2087-00255-1. The AO images were processed by replacing hot pixel values, flat fielding the array, and subtracting thermal background noise. No companions were identified in individual raw frames during the observations. However, upon stacking the images we noticed a point source to the northeast of TYC 2087-0025501. Figure 11 shows the final processed K' image. The candidate is 6.49 mag fainter than the primary star in K'. We measure an angular separation of 643 ± 10 mas and position angle $27.^{\circ}1 \pm 0.^{\circ}1$. Assuming an age of 5 Gyr, the Baraffe et al. (1998) theoretical evolutionary models predict a mass of $0.13\,M_{\odot}$ if the candidate is physically associated at a distance of 218 pc. With a proper motion of $(\mu_\alpha \cos\delta, \mu_\delta) = (-2.9, 39.8)$ mas yr^{-1} for TYC 2087-00255-1 (Høg et al. 2000), it will be possible to determine whether this candidate is a tertiary companion in less than one year with NIRC2.

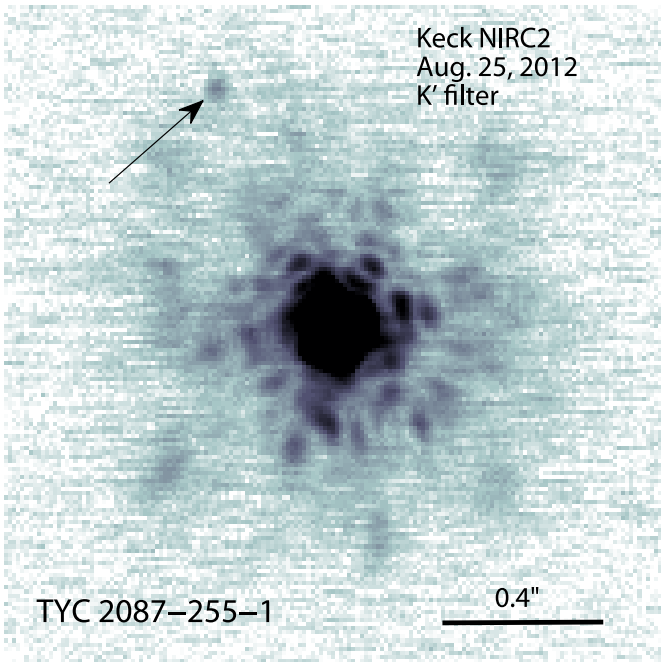

Figure 11. Keck K'-band AO image of TYC 2087-00255-1. A candidate 6.49 mag fainter than the primary star in the K band is identified. It has an angular separation of 643 ± 10 mas and position angle $27.^{\circ}1 \pm 0.^{\circ}1$ (pointed by an arrow in the plot).

(A color version of this figure is available in the online journal.)

5. DISCUSSION

5.1. Does MARVELS-4b Reside in the Low-mass Tail of the Stellar Formation Process?

The mass of BD overlaps both with low-mass stars formed from collapse/fragmentation of molecular cores and massive planetary companions formed in protoplanetary disks. It is still not clear which mechanism dominates the formation of BDs. By extrapolating the companion mass function from both the exoplanet side and low-mass star side, Grether & Lineweaver (2006) find the minimum number of companions per unit interval in log mass is 31^{+25}_{-18} $M_{\rm Jup}$. Sahlmann et al. (2011) see evidence for a bimodal distribution in BD masses, with the gap between 25 and 45 $M_{\rm Jup}$ almost entirely devoid of objects. They suggest that the less-massive group may represent the high-mass tail of the planetary distribution. If true, the maximum mass of giant "planets" should be around 30 $M_{\rm Jup}$. The BD candidate MARVELS-4b reported in this paper has a minimum mass of 40.0 ± 2.5 $M_{\rm Jup}$, which suggests that MARVELS-4b more likely formed like stars through collapse and/or fragmentation of molecular cores.

5.2. Activity, Rapid Rotation, and Stellar Spin Evolution

TYC 2087-00255-1 is in its subgiant phase with an estimated age of ~5.5 Gyr and chromospheric Ca II HK index $\log R'_{\rm HK} = -4.58$ (see Section 3.1). Jenkins et al. (2011) have studied chromospheric activity indices for more than 850 FGK-type dwarfs and subgiant stars, and find the distribution of activity indices ($\log R'_{\rm HK}$) for their subgiant sample can be fit by a Gaussian centered around −5.14, with $\sigma = 0.06$. The activity index for TYC 2087-00255-1 is $\log R'_{\rm HK} = -4.58$, which makes it an unusually active subgiant star (see also Section 3.1).

For cool stars with $T_{\rm eff} < 6500$ K, chromospheric activity is generated through a stellar magnetic dynamo, which is related to the rotational velocity and rotation period of the star. The star's rotation period increases with age through mass loss in a magnetized wind ("magnetic braking"; Schatzman 1962; Weber & Davis 1967; Mestel 1968; Skumanich 1972; Epstein & Pinsonneault 2012), and as such, its chromospheric activity level is expected to also decay with age, a phenomenon that has been observed (Wilson 1963; Skumanich 1972; Soderblom et al. 1991). For an evolved star such as TYC 2087-00255-1, the rotation period should be relatively large, $\gtrsim$ 30 days due to magnetic braking and conservation of angular momentum as the radius expands (Skumanich 1972; Epstein & Pinsonneault 2012). However, we find the rotation period (13.16 days) is much shorter than this value. One possible explanation is that the tidal interaction with the companion has spun up the star and keeps the stellar magnetic dynamo active. In this scenario, the tidal interaction transfers orbital angular momentum into stellar rotational angular momentum. We will explore the coupled roles of radial expansion and tidal evolution, and find that the observed state is consistent with tidal theory and stellar evolution.

For a star born with $T_{\rm eff} \lesssim 6500$ K, it could develop a convective zone and lose angular momentum through "magnetic braking." So even when it rotates quickly at birth, it will spin down quickly and thus have a longer period at zero-age main sequence. While for a star born with $T_{\rm eff} \gtrsim 6500$ K, it will be fully radiative and could not lose angular momentum through "magnetic braking." Thus it will rotate much more quickly. From the evolution track in Figure 5 we could see that the effective temperature of TYC 2087-00255-1 is initially around the transition point ~6500 K, and its evolution is difficult to know a priori. If fully radiative, we expect it to rotate quickly while on the main sequence, while if convective, it would have spun down and will rotate more slowly. Here we consider both scenarios and find that we cannot rule either out, at least using a simple, coupled model for the expansion of the primary and the tidal evolution.

As star evolves, its radius expands and hence we expect the star to spin down via conservation of angular momentum. If the rotational frequency of the star is ω, then its time rate of change due to expansion is

$$\left.\frac{d\omega}{dt}\right|_{\rm exp} = -\frac{2\omega}{R}\frac{dR}{dt}. \quad (1)$$

The rate at which ω changes is therefore encapsulated in dR/dt, which we can derive from stellar evolution models. Using the "Y^2" models (Demarque et al. 2004), we fit a third-order polynomial to the radius as a function of time:

$$\frac{R_*}{R_\odot} = 1.0275 + 0.1661t' - 0.0619t'^2 + 0.01147t'^3, \quad (2)$$

where t' is the age of the star in Gyr. Differentiating with respect to t' we find

$$\frac{dR_*}{dt'} = 0.1661 - 0.1238t' + 0.03441t'^2, \quad (3)$$

from which we can solve Equation (1).

The tidal evolution is considerably more complicated as it depends on many more parameters, as well as the tidal model employed. Here we use the "constant-phase-lag" (CPL) model as described in Ferraz-Mello et al. (2008). This widely used model assumes a constant phase offset between the location of the companion and the tidal bulge. The magnitude of the phase lag is $\frac{1}{2Q}$, where Q is the "tidal quality factor." Different values of Q have been proposed to explain tidal evolution of different systems (10^7 in Zahn 1989; 10^5 in Meibom & Mathieu 2005; 10^6–10^7 in Schlaufman et al. 2010; 10^8–10^9 in Penev et al. 2011). The speed of the evolution is also a function of the Love number of degree two, k_2, which is a measure of the height of the tidal bulge. Rather than reproduce the set of six coupled differential equations that comprises the CPL model, the reader is referred to Ferraz-Mello et al. (2008). Other tidal models exist (e.g., Hut 1981; Leconte et al. 2010; Hansen 2010) that make qualitatively different assumptions. As we are only interested in demonstrating that the observed configuration is consistent with tidal theory, we limit our scope to the CPL model. We use the numerical methods outlined in Appendix E of Barnes et al. (2012).

We can use the best-fit parameters in the CPL model, but we also must set Q and k_2, and the moment of inertia constant, or "radius of gyration" r_g. A wide range of values have been proposed for Q, with 10^6 being a standard choice (e.g., Jackson et al. 2008, 2009). We set k_2 to 0.5, which is arbitrary since the tidal evolution actually depends on the quotient of Q and k_2, and currently we cannot disentangle the two. We set R_g to 0.35, consistent with theoretical expectations for solar-like stars (Claret & Gimenez 1990). We assume the companion is tidally locked, use its minimum mass, and has a radius of 1 $R_{\rm Jup}$. We set both bodies' obliquities to 0. With these choices, we may integrate the tidal evolution of the system forward, tracking the spins, obliquities, orbital period, and orbital eccentricity.

Because the stellar rotational frequency depends on both its internal and tidal evolution, we include both effects in our model.

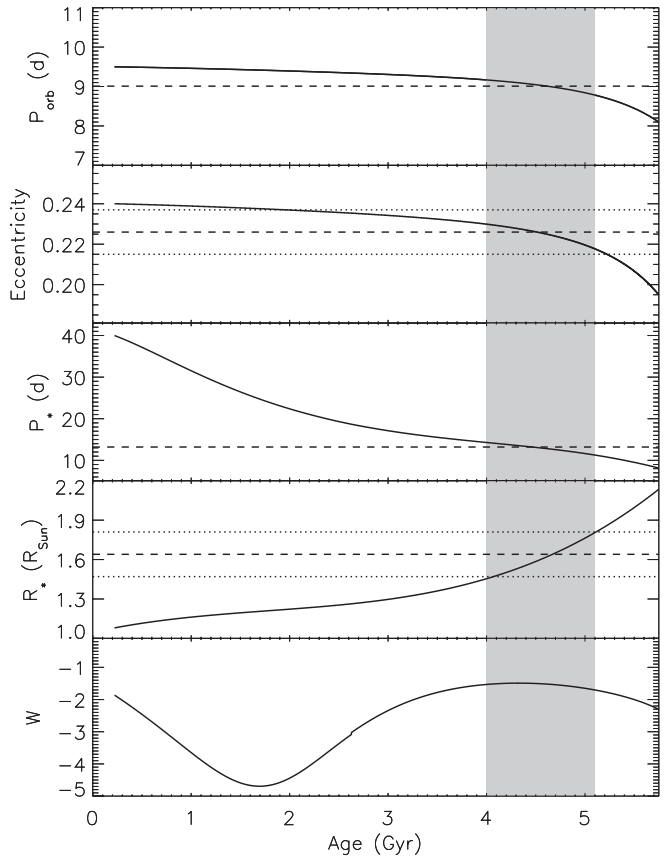

Figure 12. Evolution of various properties of the MARVELS-4 system assuming a slow initial rotation period for the primary. Top: orbital period. Top middle: eccentricity. Middle: primary's rotation period. Bottom middle: primary radius. Bottom: ratio of the time rate of change of the primary's spin period from tides to that from expansion, cf. Equation (4).

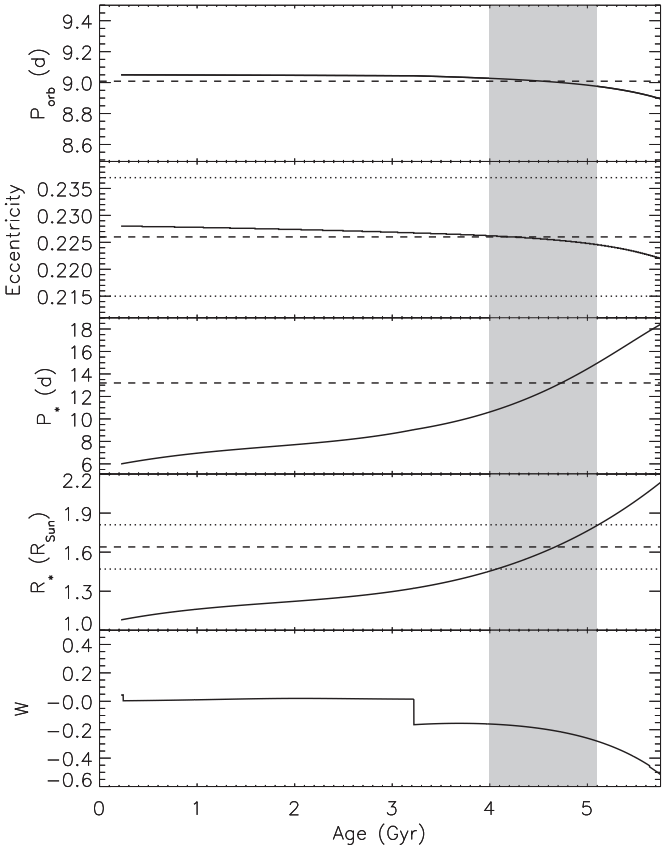

Figure 13. Evolution of various properties of the MARVELS-4 system assuming a fast initial rotation period for the primary. The format is the same as Figure 12.

Furthermore, we assume that both effects act independently, i.e., no feedbacks are present. This sort of coupling has been applied to stellar binaries before (Zahn & Bouchet 1989; Khaliullin & Khaliullina 2011; Gómez Maqueo Chew et al. 2012), but this may be the first time it has been done for a star with a BD companion.

We first consider the convective case, i.e., slow initial rotation. In Figure 12, we show one plausible history for this system. We start the integration at an age of 221 Myr when the star is on the main sequence, at which point the "Y^2" model (Demarque et al. 2004) predicts a radius of 1.08 $R_\odot$. The orbit begins with a period of 9.5 days, and an eccentricity of 0.24. The initial stellar rotation period is 40 days. We set the stellar Q to 4×10^6. Based on the radial evolution and the observed uncertainties in radius, we estimate the age of the system to be between 4 and 5.1 Gyr, and with a nominal age of 4.75 Gyr, corresponding to the best-fit radius of 1.64 $R_\odot$. This interval is shaded gray. This age estimate is different from that in Section 3.3, which is estimated from $T_{\rm eff}$ and $\log(g)$ on the H-R diagram. We also considered a wider range of configurations and find that, for plausible primary spin periods, the primary's Q must lie in the range 3×10^6–6×10^6 in order to produce a system consistent with the observations.

In the top panel, the evolution of the orbital period $P_{\rm orb}$ is shown by the solid curve. The dashed curve is the best-fit orbit, whose uncertainty is less than the curve thickness. The next panel down shows the eccentricity evolution. The line styles are the same as before, but now the 1σ observational uncertainty in e is denoted by the horizontal dotted lines. Next is the stellar rotation period, shown in the same format as the previous panels. Fourth is the evolution of the stellar radius, as given by the fit in Equation (2). Note that all these parameters pass through their best-fit values at our nominal age estimate.

The final panel shows the ratio of the stellar spin evolution from tides to that from radial expansion (Equation (1)),

$$W \equiv \frac{\frac{d\omega}{dt}|_{\rm tides}}{\frac{d\omega}{dt}|_{\rm exp}}, \quad (4)$$

where the denominator is the time rate of change of the rotational frequency due to tides. The bottom panel of Figure 12 shows the evolution of W. Although W evolves, it is always (1) negative and (2) more negative than -1. These features indicate that the tidal torques oppose the radial expansion, and dominate. Therefore, the star is spinning up, and will continue to do so until it becomes tidally locked. (The discontinuity at 2.6 Gyr is due to passage through the 2:1 spin-orbit resonance.)

We now turn to the possibility that the primary's rotation was initially fast. At first glance, it may appear that the observed system is inconsistent with such a history because the primary's rotation period is currently longer than the orbital period, implying the system has passed through the 1:1 spin-orbit resonance. In that case, the primary may have become tidally locked. However, if the expansion is rapid enough, and/or the tidal Q large enough, the primary could pass through this state and avoid permanent capture. In Figure 13, we show such a configuration. In this case, the primary's rotation period is initially six days, the eccentricity is 0.228, the primary's rotation

period is six days, and its tidal Q is 3×10^7. As before the model predicts a system that could evolve to the observed state.

The evolution of W shows the complex evolution that may have occurred. Initially $W > 0$, meaning that both tides and expansion act in the same direction, increasing the rotational period in this case. Very quickly the system passes through the 3:2 spin-orbit resonance and the phase lags change, producing the sudden drop in W. For the next 2 Gyr W increases slightly because the orbit is shrinking and increasing the tidal torques. As the primary approaches the 1:1 resonance, the torque decreases and W decreases accordingly. At 3.2 Gyr, the primary passes through the 1:1 resonance and now the tides act to speed up the rotation and hence W drops to less than 0. Right after the resonance crossing, the tidal torques are weaker, because the rotation is close to the equilibrium value (the orbital period). However, as the primary continues to expand and slow down, the disparity increases and the tidal torques grow larger. Thus, $|W|$ increases because the tidal torque increases faster than radial expansion slows the spin period. As W never becomes more negative than -1, the radial expansion dominates the evolution and rotational slowdown continues.

We therefore have two competing, plausible evolutionary models for this system. We have neglected some effects, such as magnetic breaking and coupling between the expansion and tidal evolution, and hence we do not express a preference for either model. However, given the uniqueness of this system (evolving F star, BD/low-mass stellar companion, $W \sim 0$), it may be fertile ground for further exploration and insight into tidal processes on stars with little or no convective envelope.

In Section 4.4 we have found a point source near TYC 2087-00255-1 using AO imaging. Interactions between MARVELS-4b and the tertiary may serve the purpose of bringing MARVELS-4b from its birth place to a tight orbit in the early history of this system through Kozai–Lidov mechanism if the tertiary is indeed associated with TYC 2087-00255-1 and if the initial mutual orbit inclination angle between MARVELS-4b and the tertiary is $39.^\circ2 \lesssim \delta_{23} \lesssim 141.^\circ8$ (Kozai 1962; Lidov 1962). This mechanism combined with tidal friction have been proposed to explain formation of close binaries in triple-star system (Mazeh & Shaham 1979; Kiseleva et al. 1998; Eggleton & Kiseleva-Eggleton 2001; Eggleton & Kisseleva-Eggleton 2006; Tokovinin et al. 2006; Fabrycky & Tremaine 2007) and formation of close-in Jupiter mass exoplanets ("Hot Jupiters"; Wu & Murray 2003; Fabrycky & Tremaine 2007; Wu et al. 2007; Naoz et al. 2011). After MARVELS-4b has been brought to a tight orbit, tidal force from the primary takes over and MARVELS-4b follows the evolution illustrated above in Figures 12 and 13 qualitatively.

5.3. Expected Stellar RV Jitter

Starspots and motions of the stellar surface are astrophysical sources of noise that can interfere with searches for companion RV signals. These sources are commonly referred to as "jitter," first noticed by Gunn & Griffin (1979) and Lupton et al. (1987), and subsequently explored by Saar & Donahue (1997), Saar et al. (1998), Wright (2005), Lagrange et al. (2009), and Isaacson & Fischer (2010). Using the analytical relation given in Saar & Donahue (1997), we estimate the expected RV jitter for TYC 2087-00255-1 as $6.5 f^{0.9} v_{\rm rot} \sin i$, where f is the flux change in percent and $v_{\rm rot} \sin i$ is the projected rotational velocity. We have derived $v_{\rm rot} \sin i$ from our spectra using two different methods (see Section 3.4). The final combined value for $v_{\rm rot} \sin i$ is 9.9 ± 0.8 km s^{-1}. The percentage change of the stellar flux is estimated to be $f \sim 1.8$ from the SuperWASP photometry data, thus the expected RV jitter is $\sim$106 m s^{-1}.

During the joint Keplerian orbital fit to the MARVEL+SARG RV data, an RV jitter $\sim$112 m s^{-1} was needed to account for the extra noise in our RV measurements, which matches the expected jitter. However, when we use the MARVELS RV data only, we yield a "jitter" term $\sigma_{\rm jitter} = 152$ m s^{-1} in our Keplerian orbital fit, which is bigger than the expected RV "jitter" arising from the stellar activity. This implies that uncharacterized systematics remain in the MARVELS RV data, and may likely dominate the stellar RV "jitter."

6. SUMMARY

In a search through the first two years of SDSS-III MARVELS data, we discovered MARVELS-4b, a candidate BD companion to the $V \simeq 10.6$ star TYC 2087-00255-1 with a velocity semi-amplitude of $K = 3.571 \pm 0.041$ km s^{-1} and a short orbital period of 9.0090 ± 0.0004 days, yet with an eccentricity $e = 0.226 \pm 0.011$. Additional RV data from SARG observations confirm the Doppler variability. High-resolution spectroscopic observations indicate that the host star is a slightly evolved subgiant with $T_{\rm eff} = 5903 \pm 42$ K, $\log g = 4.07 \pm 0.16$, and [Fe/H] $= -0.23 \pm 0.04$, with an inferred mass of $M_* = 1.16 \pm 0.11\, M_\odot$. The minimum mass of MARVELS-4b is $40.0 \pm 2.5\, M_{\rm Jup}$, implying that it is most likely in the BD regime. A 13.16 day periodic signal is found in the SuperWASP photometry data, which is likely due to rotational modulation of starspots on the host star, and indicates that this star-BD system is not tidally synchronized. A second possible companion is found 643 ± 10 mas away from TYC 2087-00255-1 using K' AO imaging. Its association with the primary star could be verified by future proper motion measurements. Ca II H and K core emission indicates that the subgiant is chromospherically active at a level unusual for subgiants. Tidal interactions between the star and BD could have spun up the star and make it active.

Funding for the MARVELS multi-object Doppler instrument was provided by the W. M. Keck Foundation and NSF with grant AST-0705139. The MARVELS survey was partially funded by the SDSS-III consortium, NSF grant AST-0705139, NASA with grant NNX07AP14G, and the University of Florida. Funding for SDSS-III has been provided by the Alfred P. Sloan Foundation, the Participating Institutions, the National Science Foundation, and the U.S. Department of Energy Office of Science. The SDSS-III Web site is http://www.sdss3.org/. SDSS-III is managed by the Astrophysical Research Consortium for the Participating Institutions of the SDSS-III Collaboration including the University of Arizona, the Brazilian Participation Group, Brookhaven National Laboratory, University of Cambridge, Carnegie Mellon University, University of Florida, the French Participation Group, the German Participation Group, Harvard University, the Instituto de Astrofisica de Canarias, the Michigan State/Notre Dame/JINA Participation Group, Johns Hopkins University, Lawrence Berkeley National Laboratory, Max Planck Institute for Astrophysics, Max Planck Institute for Extraterrestrial Physics, New Mexico State University, New York University, Ohio State University, Pennsylvania State University, University of Portsmouth, Princeton University, the Spanish Participation Group, University of Tokyo, University of Utah, Vanderbilt University, University of Virginia, University of Washington, and Yale University.

This work is based on observations collected at Observatório do Pico dos Dias (OPD), operated by the Laboratório Nacional

de Astrofísica, CNPq, Brazil. FEROS spectra were observed at the ESO 2.2 m telescope under the ESO-ON agreement. This work has made use of observations taken with the Telescopio Nationale Galileo (TNG) operated on the island of La Palma by the Foundation Galileo Galilei, funded by the Instituto Nazionale di Astrofisica (INAF), in the Spanish Observatorio del Roque de los Muchachos of the Instituto de Astrofísica de Canarias (IAC).

This research is partially supported by funding from the Center for Exoplanets and Habitable Worlds. The Center for Exoplanets and Habitable Worlds is supported by the Pennsylvania State University, the Eberly College of Science, and the Pennsylvania Space Grant Consortium. Keivan Stassun, Leslie Hebb, and Joshua Pepper acknowledge funding support from the Vanderbilt Initiative in Data-Intensive Astrophysics (VIDA) from Vanderbilt University, and from NSF Career award AST-0349075. E.A. thanks NSF for CAREER grant 0645416. G.F.P.M. acknowledges financial support from CNPq grant No. 476909/2006-6 and FAPERJ grant No. APQ1/26/170.687/2004. L.G. acknowledges financial support provided by the PAPDRJ CAPES/FAPERJ Fellowship. J.P.W. acknowledges support from NSF Astronomy & Astrophysics Postdoctoral Fellowship AST 08-02230. L.D.F. acknowledges financial support from CAPES. R.B. acknowledges support from NSF AST grant 1108882. B.S.G. acknowledges funding support from NSF CAREER grant AST-105652.

This research has benefitted from the M, L, and T dwarf compendium housed at DwarfArchives.org (http://spider.ipac.caltech.edu/staff/davy/ARCHIVE/index.shtml) and maintained by Chris Gelino, Davy Kirkpatrick, and Adam Burgasser.

We have used data from the WASP public archive in this research. The WASP consortium comprises of the University of Cambridge, Keele University, University of Leicester, The Open University, The Queen's University Belfast, St. Andrews University and the Isaac Newton Group. Funding for WASP comes from the consortium universities and from the UK's Science and Technology Facilities Council.

This publication makes use of data products from the Two Micron All Sky Survey, which is a joint project of the University of Massachusetts and the Infrared Processing and Analysis Center/California Institute of Technology, funded by the National Aeronautics and Space Administration and the National Science Foundation.

This publication makes use of data products from the Wide-field Infrared Survey Explorer, which is a joint project of the University of California, Los Angeles, and the Jet Propulsion Laboratory/California Institute of Technology, funded by the National Aeronautics and Space Administration.

REFERENCES

Alibert, Y., Mordasini, C., Benz, W., & Winisdoerffer, C. 2005, A&A, 434, 343
André, P., Ward-Thompson, D., & Greaves, J. 2012, Sci, 337, 69
Baraffe, I., Chabrier, G., Allard, F., & Hauschildt, P. H. 1998, A&A, 337, 403
Barnes, R., Mullins, K., Goldblatt, C., et al. 2012, AsBio, in press (arXiv:1203.5104)
Basri, G., Marcy, G. W., & Graham, J. R. 1996, ApJ, 458, 600
Burrows, A., Hubbard, W. B., Lunine, J. I., & Liebert, J. 2001, RvMP, 73, 719
Burrows, A., Marley, M., Hubbard, W. B., et al. 1997, ApJ, 491, 856
Butters, O. W., West, R. G., Anderson, D. R., et al. 2010, A&A, 520, L10
Chabrier, G. 2002, ApJ, 567, 304
Chabrier, G., & Baraffe, I. 2000, ARA&A, 38, 337
Claret, A., & Gimenez, A. 1990, Ap&SS, 169, 215
Collier Cameron, A., Pollacco, D., Street, R. A., et al. 2006, MNRAS, 373, 799
Cox, A. N. (ed.) 2000, Allen's Astrophysical Quantities (4th ed.; New York: Springer)
Cutri, R. M., Skrutskie, M. F., van Dyk, S., et al. 2003, The IRSA 2MASS All-Sky Point Source Catalog, NASA/IPAC Infrared Science Archive
Cutri, R. M., Wright, E. L., Conrow, T., et al. 2012, ViZieR On-line Data Catalog: II/307
Delfosse, X., Forveille, T., Sgransan, D., et al. 2000, A&A, 364, 217
Demarque, P., Woo, J., Kim, Y., & Yi, S. K. 2004, ApJS, 155, 667
Eggleton, P. P., & Kiseleva-Eggleton, L. 2001, ApJ, 562, 1012
Eggleton, P. P., & Kisseleva-Eggleton, L. 2006, Ap&SS, 304, 75
Eisenstein, D. J., Weinberg, D. H., Agol, E., et al. 2011, AJ, 142, 72
Epstein, C. R., & Pinsonneault, M. H. 2012, arXiv:1203.1618
Erskine, D. J., & Ge, J. 2000, in ASP Conf. Ser. 195, Imaging the Universe in Three Dimensions, ed. W. van Breugel & J. Bland-Hawthorn (San Francisco, CA: ASP), 501
Fabrycky, D., & Tremaine, S. 2007, ApJ, 669, 1298
Femenía, B., Rebolo, R., Prez-Prieto, J. A., et al. 2011, MNRAS, 413, 1524
Ferraz-Mello, S., Rodríguez, A., & Hussmann, H. 2008, CeMDA, 101, 171
Fleming, S. W., Ge, J., Barnes, R., et al. 2012, AJ, 144, 72
Fleming, S. W., Ge, J., Mahadevan, S., et al. 2010, ApJ, 718, 1186
Ford, E. B. 2006, ApJ, 642, 505
Ford, E. B., Havlickova, M., & Rasio, F. A. 2001, Icar, 150, 303
Ge, J. 2002, ApJ, 571, L165
Ge, J., Lee, B., de Lee, N., et al. 2009, Proc. SPIE, 7440, 74400L
Ge, J., Mahadevan, S., Lee, B., et al. 2008, in ASP Conf. Ser. 398, Extreme Solar Systems, ed. D. Fischer, F. A. Rasio, S. E. Thorsett, & A. Wolszczan (San Francisco, CA: ASP), 449
Ghez, A. M., Salim, S., Weinberg, N. N., et al. 2008, ApJ, 689, 1044
Ghezzi, L., Cunha, K., Schuler, S. C., & Smith, V. V. 2010a, ApJ, 725, 721
Ghezzi, L., Cunha, K., Smith, V. V., et al. 2010b, ApJ, 720, 1290
Gizis, J. E., Kirkpatrick, J. D., Burgasser, A., et al. 2001, ApJ, 551, L163
Gómez Maqueo Chew, Y., Stassun, K. G., Prša, A., et al. 2012, ApJ, 745, 58
Gratton, R. G., Bonanno, G., Bruno, P., et al. 2001, ExA, 12, 107
Gregory, P. C. 2007, MNRAS, 381, 1607
Grether, D., & Lineweaver, C. H. 2006, ApJ, 640, 1051
Gunn, J. E., & Griffin, R. F. 1979, AJ, 84, 752
Gunn, J. E., Siegmund, W. A., Mannery, E. J., et al. 2006, AJ, 131, 2332
Hansen, B. M. S. 2010, ApJ, 723, 285
Hauschildt, P. H., Allard, F., & Baron, E. 1999, ApJ, 512, 377
Hennebelle, P., & Chabrier, G. 2008, ApJ, 684, 395
Henry, T. J. 2004, in ASP Conf. Ser. 318, Spectroscopically and Spatially Resolving the Components of the Close Binary Stars, ed. R. W. Hilditch, H. Hensberge, & K. Pavlovski (San Francisco, CA: ASP), 159
Henry, T. J., Franz, O. G., Wasserman, L. H., et al. 1999, ApJ, 512, 864
Høg, E., Fabricius, C., Makarov, V. V., et al. 2000, A&A, 355, L27
Hut, P. 1981, A&A, 99, 126
Isaacson, H., & Fischer, D. A. 2010, ApJ, 725, 875
Jackson, B., Barnes, R., & Greenberg, R. 2009, ApJ, 698, 1357
Jackson, B., Greenberg, R., & Barnes, R. 2008, ApJ, 678, 1396
Jenkins, J. S., Jones, H. R. A., Pavlenko, Y., et al. 2008, A&A, 485, 571
Jenkins, J. S., Murgas, F., Rojo, P., et al. 2011, A&A, 531, A8
Kane, S. R., & von Braun, K. 2008, ApJ, 689, 492
Kaufer, A., Stahl, O., Tubbesing, S., et al. 1999, Msngr, 95, 8
Khaliullin, K. F., & Khaliullina, A. I. 2011, MNRAS, 411, 2804
Kharchenko, N. V., & Roeser, S. 2009, yCat, 1280, 0
Kiseleva, L. G., Eggleton, P. P., & Mikkola, S. 1998, MNRAS, 300, 292
Kozai, Y. 1962, AJ, 67, 591
Lafrenière, D., Doyon, R., Marois, C., et al. 2007, ApJ, 670, 1367
Lagrange, A., Desort, M., Galland, F., Udry, S., & Mayor, M. 2009, A&A, 495, 335
Leconte, J., Chabrier, G., Baraffe, I., & Levrard, B. 2010, A&A, 516, A64
Lee, B. L., Ge, J., Fleming, S. W., et al. 2011, ApJ, 728, 32
Lidov, M. L. 1962, P&SS, 9, 719
Luhman, K. L., Rieke, G. H., Young, E. T., et al. 2000, ApJ, 540, 1016
Lupton, R. H., Gunn, J. E., & Griffin, R. F. 1987, AJ, 93, 1114
Lyra, W., & Porto de Mello, G. F. 2005, A&A, 431, 329
Mamajek, E. 2010, A Modern Dwarf Stellar Effective Temperature Scale Based on 17842 Teff and MK Spectral Type Pairs, http://www.pas.rochester.edu/~emamajek/Teff_SpT_table.txt
Mamajek, E. E., & Hillenbrand, L. A. 2008, ApJ, 687, 1264
Marcy, G. W., & Butler, R. P. 2000, PASP, 112, 137
Mayor, M., & Queloz, D. 1995, Natur, 378, 355
Mazeh, T., & Shaham, J. 1979, A&A, 77, 145
Meibom, S., & Mathieu, R. D. 2005, ApJ, 620, 970
Mestel, L. 1968, MNRAS, 138, 359
Metchev, S. A., & Hillenbrand, L. A. 2004, ApJ, 617, 1330
Metchev, S. A., & Hillenbrand, L. A. 2009, ApJS, 181, 62

Mordasini, C., Alibert, Y., Benz, W., & Naef, D. 2008, in ASP Conf. Ser. 398, Extreme Solar Systems, ed. D. Fischer, F. A. Rasio, S. E. Thorsett, & A. Wolszczan (San Francisco, CA: ASP), 235
Morrissey, P., Conrow, T., Barlow, T. A., et al. 2007, ApJS, 173, 682
Nakajima, T., Oppenheimer, B. R., Kulkarni, S. R., et al. 1995, Natur, 378, 463
Naoz, S., Farr, W. M., Lithwick, Y., Rasio, F. A., & Teyssandier, J. 2011, Natur, 473, 187
Oppenheimer, B. R., Kulkarni, S. R., Matthews, K., & Nakajima, T. 1995, Sci, 270, 1478
Oscoz, A., et al. 2008, Proc. SPIE, 7014, 701447-1
Padoan, P., & Nordlund, Å. 2004, ApJ, 617, 559
Pasquini, L., & Pallavicini, R. 1991, A&A, 251, 199
Patel, S. G., Vogt, S. S., Marcy, G. W., et al. 2007, ApJ, 665, 744
Penev, K., Barranco, J., & Sasselov, D. 2011, ApJ, 734, 118
Pollacco, D. L., Skillen, I., Collier Cameron, A., et al. 2006, PASP, 118, 1407
Prugniel, P., & Soubiran, C. 2001, A&A, 369, 104
Rebolo, R., Martin, E. L., Basri, G., Marcy, G. W., & Zapatero-Osorio, M. R. 1996, ApJ, 469, L53
Rebolo, R., Zapatero Osorio, M. R., & Martín, E. L. 1995, Natur, 377, 129
Reid, I. N., & Metchev, S. A. 2008, in Exoplanets, ed. J. Mason (Chichester: Praxis), 115
Saar, S. H., Butler, R. P., & Marcy, G. W. 1998, ApJ, 498, L153
Saar, S. H., & Donahue, R. A. 1997, ApJ, 485, 319
Sahlmann, J., Ségransan, D., Queloz, D., et al. 2011, A&A, 525, A95
Schatzman, E. 1962, AnAp, 25, 18
Schlaufman, K. C., Lin, D. N. C., & Ida, S. 2010, ApJ, 724, L53
Schlegel, D. J., Finkbeiner, D. P., & Davis, M. 1998, ApJ, 500, 525
Skumanich, A. 1972, ApJ, 171, 565
Soderblom, D. R., Duncan, D. K., & Johnson, D. R. H. 1991, ApJ, 375, 722
Spiegel, D. S., Burrows, A., & Milsom, J. A. 2011, ApJ, 727, 57
Tokovinin, A., Thomas, S., Sterzik, M., & Udry, S. 2006, A&A, 450, 681
Torres, G., Andersen, J., & Giménez, A. 2010, A&ARv, 18, 67
Valenti, J. A., & Fischer, D. A. 2005, ApJS, 159, 141
Valenti, J. A., & Piskunov, N. 1996, A&AS, 118, 595
van Eyken, J. C., Ge, J., & Mahadevan, S. 2010, ApJS, 189, 156
Vogt, S. S., Butler, R. P., Marcy, G. W., et al. 2002, ApJ, 568, 352
Wang, J., Ge, J., Jiang, P., & Zhao, B. 2011, ApJ, 738, 132
Wang, J., Ge, J., Wan, X., De Lee, N., & Lee, B. 2012b, PASP, 124, 1159
Wang, J., Ge, J., Wan, X., Lee, B., & De Lee, N. 2012a, PASP, 124, 598
Weber, E. J., & Davis, L., Jr. 1967, ApJ, 148, 217
Wilson, O. C. 1963, ApJ, 138, 832
Wisniewski, J. P., Ge, J., Crepp, J. R., et al. 2012, AJ, 143, 107
Wittenmyer, R. A., Endl, M., Cochran, W. D., et al. 2009, AJ, 137, 3529
Wright, E. L., Eisenhardt, P. R. M., Mainzer, A. K., et al. 2010, AJ, 140, 1868
Wright, J. T. 2005, PASP, 117, 657
Wu, Y., & Murray, N. 2003, ApJ, 589, 605
Wu, Y., Murray, N. W., & Ramsahai, J. M. 2007, ApJ, 670, 820
Xia, F., & Fu, Y.-N. 2010, ChA&A, 34, 277
Xia, F., Ren, S., & Fu, Y. 2008, Ap&SS, 314, 51
Zahn, J.-P. 1989, A&A, 220, 112
Zahn, J.-P., & Bouchet, L. 1989, A&A, 223, 112